Supplement of Atmos. Chem. Phys., 20, 1941–1959, 2020
https://doi.org/10.5194/acp-20-1941-2020-supplement

Atmospheric Chemistry and Physics
Open Access
EGU

Supplement of

Terpenes and their oxidation products in the French Landes forest: insights from Vocus PTR-TOF measurements

Haiyan Li et al.

Correspondence to: Haiyan Li (haiyan.li@helsinki.fi) and Matthieu Riva (matthieu.riva@ircelyon.univ-lyon1.fr)

Detection of the high $C_4H_9^+$ signals

One possible contribution to the detected $C_4H_9^+$ could be the protonated butene, which is emitted by biogenic or anthropogenic sources (Goldstein et al., 1996; Hellén et al., 2006; Zhu et al., 2017). In addition, $C_4H_9^+$ ions are very common fragments of many VOCs in PTR instruments and the peaks are prominent in the mass spectra (Pagonis et al., 2019). The fragmentation of butanol also produces significant $C_4H_9^+$ signals. Like many other alcohols, butanol can easily lose an OH during ionization in PTR sources (Spanel and Smith, 1997). During the measurements at the Station for Measuring Ecosystem-Atmosphere Relations (SMEAR II) site in Hyytiälä, Finland, Schallhart et al. (2018) concluded that $C_4H_9^+$ signal detected by PTR-TOF mainly came from butanol used by aerosol instruments, i.e., condensation particle counters (CPCs). In this study, CPCs using butanol to measure the particle concentration were also deployed at the site. While the exhaust air emitted from these collocated instruments was filtered using charcoal denuder, we cannot exclude the contribution of butanol to the identified $C_4H_9^+$ signal. The spiky peaks in the time series of $C_4H_9^+$ compound also indicated the influence of butanol (Fig. S19). Finally, the green leaf volatiles (GLV), a group of six-carbon aldehyde, alcohols and their esters which can be directly released by the plants, have been found to fragment at *m/z* 57 inside the PTR instruments (Rinne et al., 2005; Pang, 2015) and may also contribute to the observed $C_4H_9^+$ signal.

Calculation of the steady-state OH concentration from alkene ozonolysis

If the competition between OH production and removal processes leads to a steady station of OH formation, the OH concentration can be calculated using the following equation (Dusanter et al., 2008):

$$[OH]ss = \frac{k_{O3+VOC}\alpha[O3][alkene]}{k_{OH+VOC}[alkene] + k_{OH+O3}[O3]}$$

where k_{O3+VOC} is the rate constant for O_3+alkene reaction with an OH yield of α, k_{OH+VOC} is the rate constant for OH+alkene reaction, k_{OH+O3} is the rate constant for OH+ O_3 reaction. The rate constant of OH and O_3 reactions was obtained from Atkinson et al. (1992). At night, alkene concentrations in the Landes forest were dominated by monoterpenes, mainly α- and β-pinene (Riba et al., 1987; Simon et al., 1994). For the calculation of OH concentration, the loss of OH from reaction with O_3 was neglected, as it was much smaller than the loss of OH due to its reaction with monoterpenes (Gill and Hites, 2002). The rate constant of O_3 and monoterpene reactions was taken from Hakola et al. (2012), and the OH formation yield from O_3 and monoterpene reactions was obtained from Alicke et al. (2003). Finally, we assumed the equal contribution of α- and β-pinene to OH formation through alkene ozonolysis in this study. Hence, using an O_3 concentration of ~20 ppb at 8 pm, the OH concentration is estimated to be 0.012 ppt.

References

Goldstein, A. H., Fan, S. M., Goulden, M. L., Munger, J. W., and Wofsy, S. C.: Emissions of ethene, propene, and 1-butene by a midlatitude forest, Journal of Geophysical Research: Atmospheres, 101, 9149-9157, 10.1029/96JD00334, 1996.

Hellén, H., Hakola, H., Pystynen, K.-H., Rinne, J., and Haapanala, S.: C2-C10 hydrocarbon emissions from a boreal wetland and forest floor, Biogeosciences, 3, 167–174, https://doi.org/10.5194/bg-3-167-2006, 2006.

Zhu, Y., Yang, L., Kawamura, K., Chen, J., Ono, K., Wang, X., Xue, L., and Wang, W.: Contributions and source identification of biogenic and anthropogenic hydrocarbons to secondary organic aerosols at Mt. Tai in 2014, Environ Pollut, 220, 863-872, https://doi.org/10.1016/j.envpol.2016.10.070, 2017.

Pagonis, D., Sekimoto, K., and de Gouw, J.: A Library of Proton-Transfer Reactions of H3O+ Ions Used for Trace Gas Detection, Journal of The American Society for Mass Spectrometry, 30, 1330-1335, 10.1007/s13361-019-02209-3, 2019.

Spanel, P., and Smith, D.: SIFT studies of the reactions of H3O+, NO+ and O2+ with a series of alcohols, International Journal of Mass Spectrometry and Ion Processes, 167-168, 375-388, https://doi.org/10.1016/S0168-1176(97)00085-2, 1997.

Schallhart, S., Rantala, P., Kajos, M. K., Aalto, J., Mammarella, I., Ruuskanen, T. M., and Kulmala, M.: Temporal variation of VOC fluxes measured with PTR-TOF above a boreal forest, Atmos. Chem. Phys., 18, 815-832, 10.5194/acp-18-815-2018, 2018.

Rinne, J., Ruuskanen, T. M., Reissell, A., Taipale, R., Hakola, H., and Kulmala, M.: On-line PTR-MS measurements of atmospheric concentrations of volatile organic compounds in a European boreal forest ecosystem, Boreal Environ. Res., 10, 425–436, 2005.

Pang, X.: Biogenic volatile organic compound analyses by PTR-TOF-MS: Calibration, humidity effect and reduced electric field dependency, Journal of Environmental Sciences, 32, 196-206, https://doi.org/10.1016/j.jes.2015.01.013, 2015.Dusanter, S., Vimal, D., and Stevens, P. S.: Technical note: Measuring tropospheric OH and HO2 by laser-induced fluorescence at low pressure. A comparison of calibration techniques, Atmos. Chem. Phys., 8, 321–340, https://doi.org/10.5194/acp-8-321-2008, 2008.

Atkinson, R., Baulch, D. L., Cox, R. A., Hampson, R. F., Kerr, J. A., and Troe, J.: Evaluated Kinetic and Photochemical Data for Atmospheric Chemistry: Supplement IV. IUPAC Subcommittee on Gas Kinetic Data Evaluation for Atmospheric Chemistry, Journal of Physical and Chemical Reference Data, 21, 1125-1568, 10.1063/1.555918, 1992.

Riba, M. L., Tathy, J. P., Tsiropoulos, N., Monsarrat, B., and Torres, L.: Diurnal variation in the concentration of α- and β-pinene in the landes forest (France), Atmospheric Environment (1967), 21, 191-193, https://doi.org/10.1016/0004-6981(87)90285-X, 1987.

Simon, V., Clement, B., Riba, M. L., and Torres, L.: The Landes experiment: monoterpenes emitted from maritime pine, J. Geophys. Res., 99, 16501–16510, 1994.

Gill, K. J., and Hites, R. A.: Rate Constants for the Gas-Phase Reactions of the Hydroxyl Radical with Isoprene, α- and β-Pinene, and Limonene as a Function of Temperature, The Journal of Physical Chemistry A, 106, 2538-2544, 10.1021/jp013532q, 2002.

Hakola, H., Hellén, H., Hemmilä, M., Rinne, J., and Kulmala, M.: In situ measurements of volatile organic compounds in a boreal forest, Atmos. Chem. Phys., 12, 11665-11678, 10.5194/acp-12-11665-2012, 2012.

Alicke, B., Geyer, A., Hofzumahaus, A., Holland, F., Konrad, S., Pätz, H. W., Schäfer, J., Stutz, J., Volz-Thomas, A., and Platt, U.: OH formation by HONO photolysis during the BERLIOZ experiment, Journal of Geophysical Research: Atmospheres, 108, PHO 3-1-PHO 3-17, 10.1029/2001JD000579, 2003.

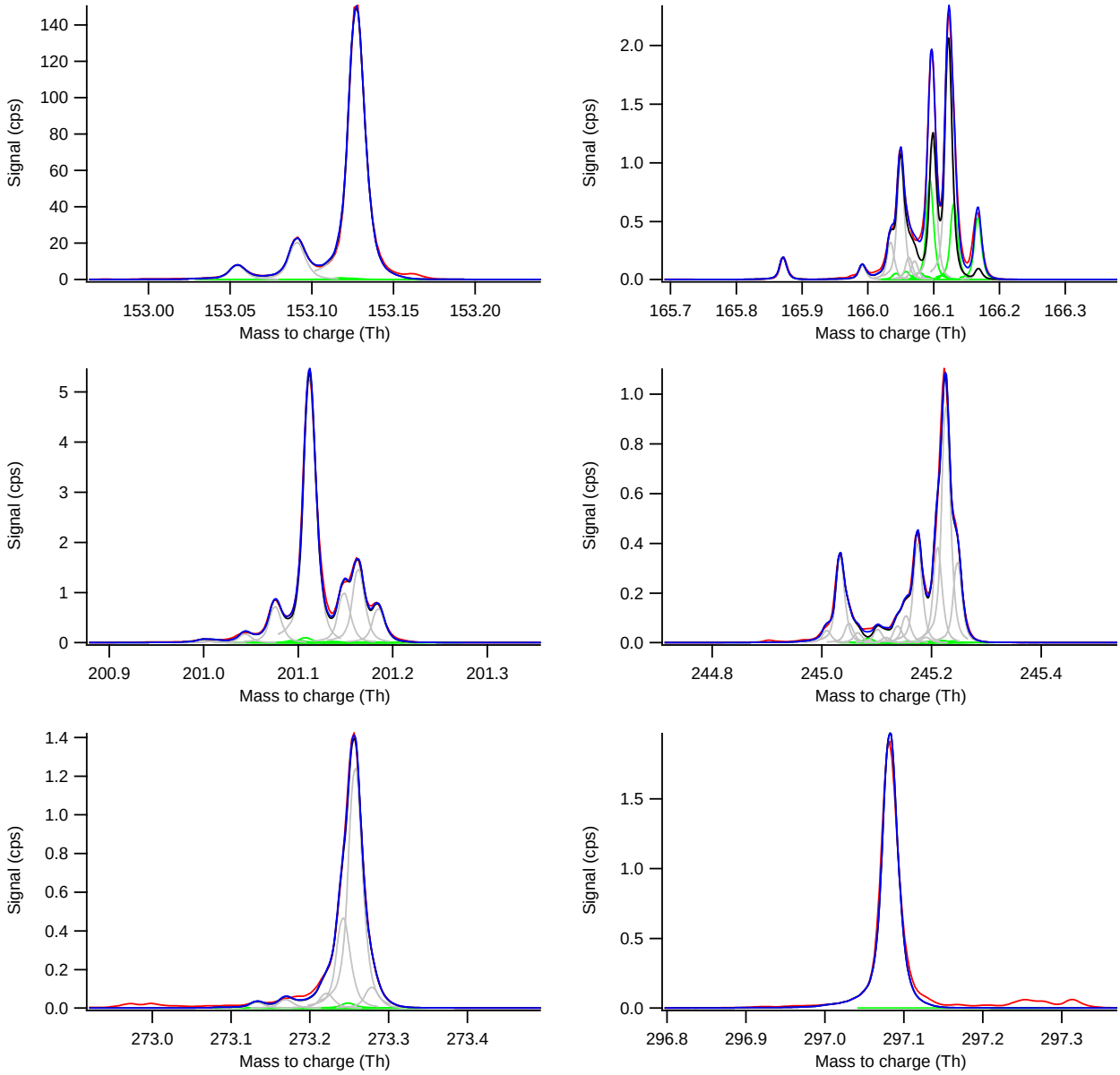

Figure S1. Examples of peak identification with the LTOF mass analyzer.

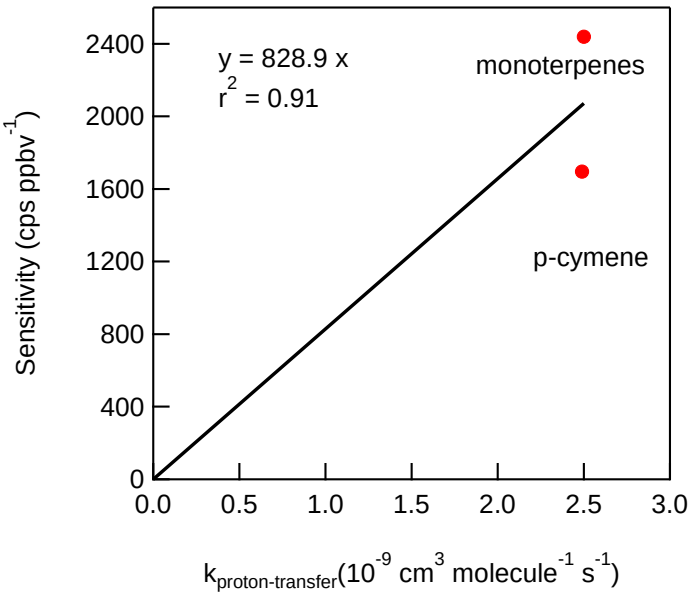

Figure S2. The built empirical relationship between the sensitivities and the proton-transfer reaction rate coefficients (k) using the calibrated data of monoterpenes and *p*-cymene: Sensitivity (cps ppb^{-1}) = 828.9 × k.

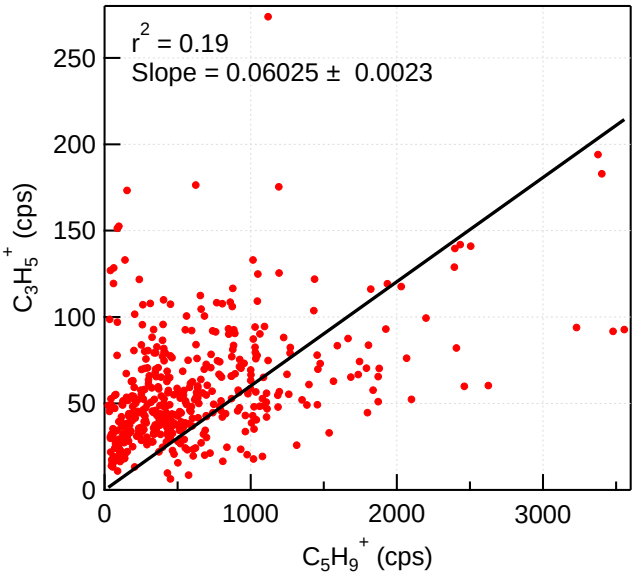

Figure S3. Correlation of the time variations between $C_3H_5^+$ and $C_5H_9^+$ signals.

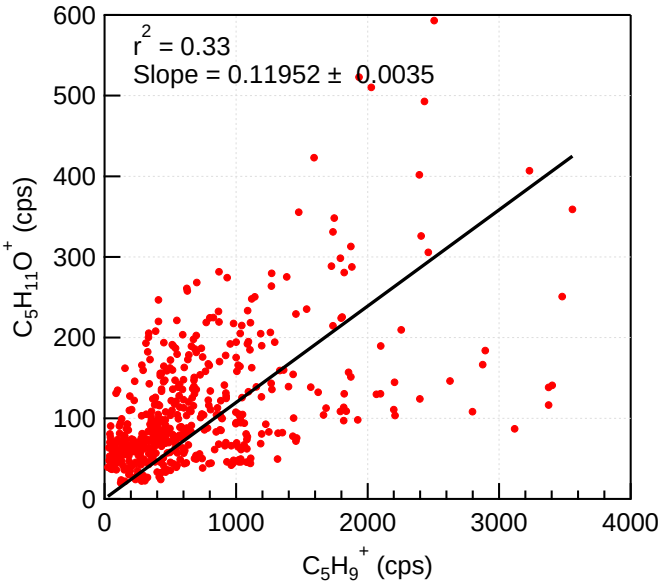

Figure S4. Correlation of the time variations between $C_5H_{11}O^+$ and $C_5H_9^+$ signals.

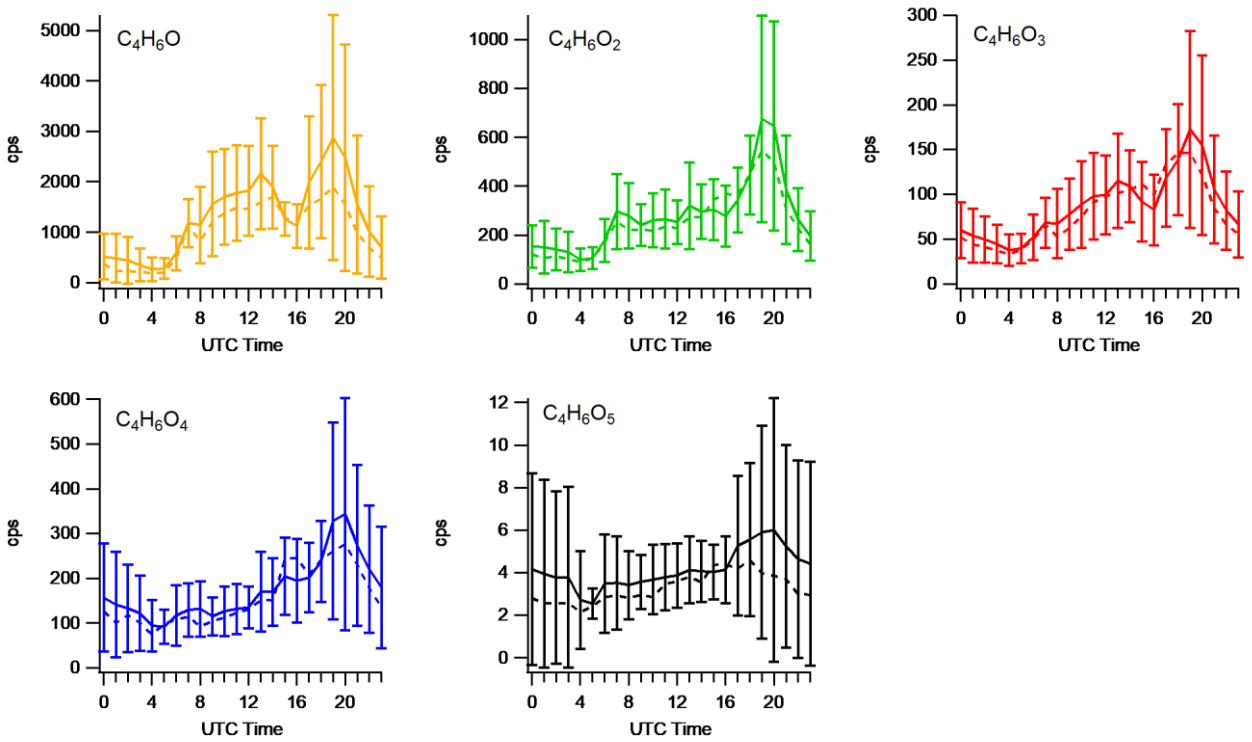

Figure S5. Diurnal patterns of non-nitrate isoprene oxidation products: (a) C_4H_6O, (b) $C_4H_6O_2$, (c) $C_4H_6O_3$, (d) $C_4H_6O_4$, and (e) $C_4H_6O_5$.

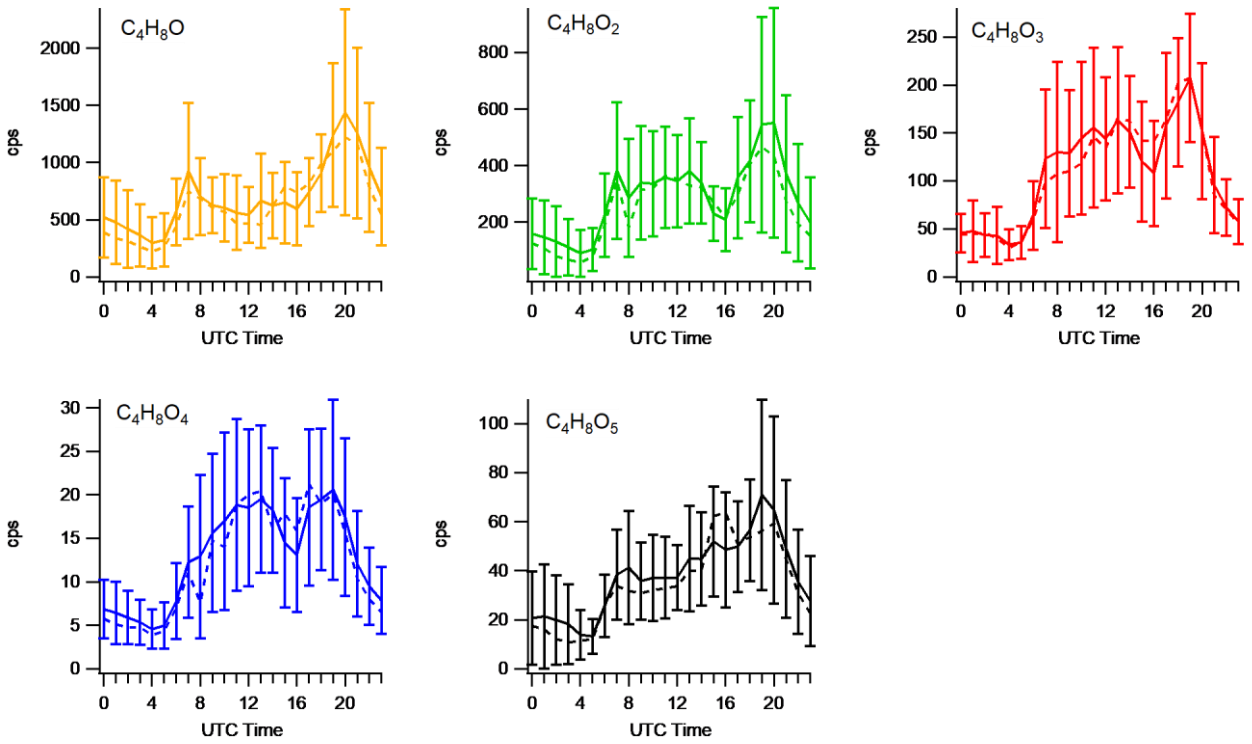

Figure S6. Diurnal patterns of non-nitrate isoprene oxidation products: (a) C_4H_8O, (b) $C_4H_8O_2$, (c) $C_4H_8O_3$, (d) $C_4H_8O_4$, and (e) $C_4H_8O_5$.

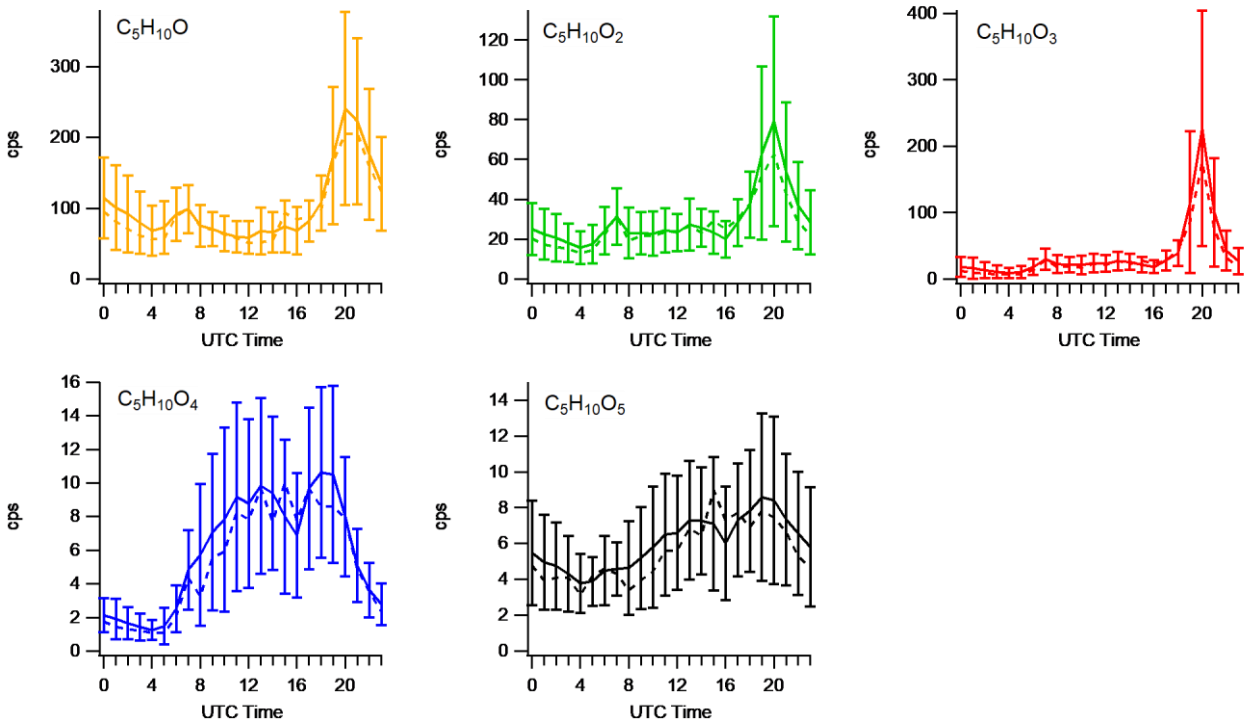

Figure S7. Diurnal patterns of non-nitrate isoprene oxidation products: (a) $C_5H_{10}O$, (b) $C_5H_{10}O_2$, (c) $C_5H_{10}O_3$, (d) $C_5H_{10}O_4$, and (e) $C_5H_{10}O_5$.

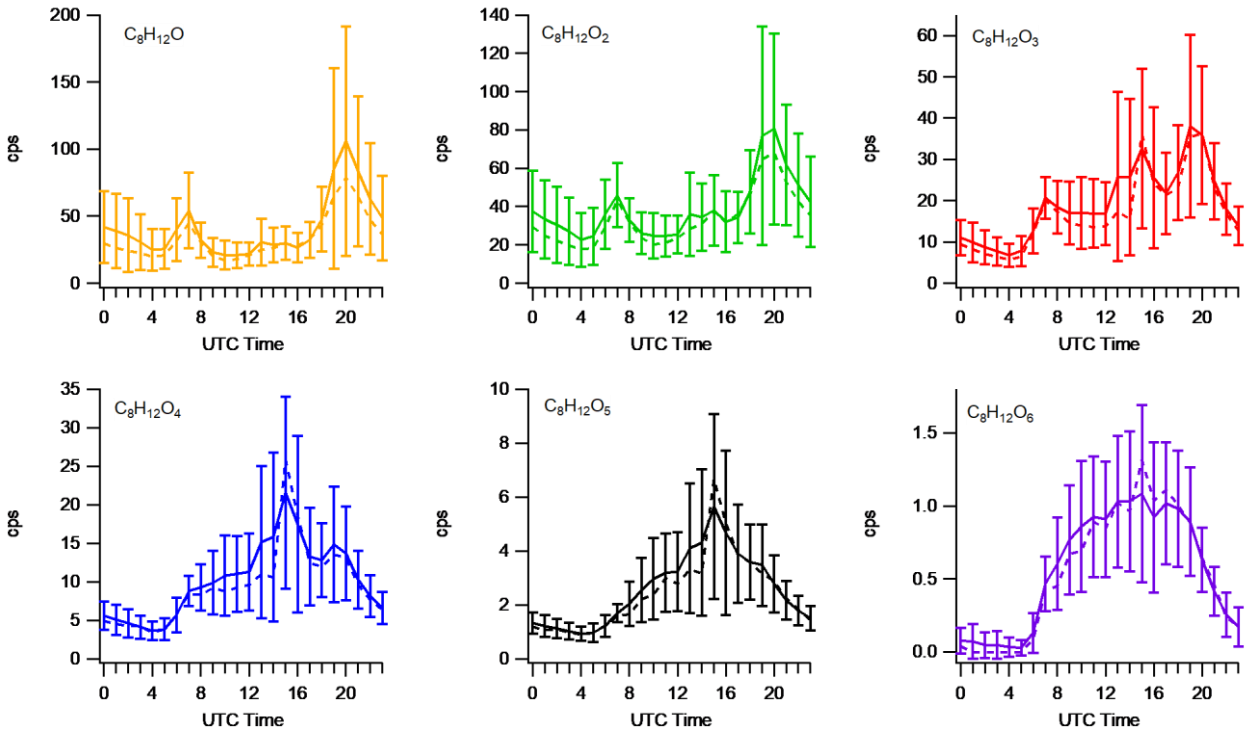

Figure S8. Diurnal patterns of non-nitrate monoterpene oxidation products: (a) $C_8H_{12}O$, (b) $C_8H_{12}O_2$, (c) $C_8H_{12}O_3$, (d) $C_8H_{12}O_4$, (e) $C_8H_{12}O_5$, and (f) $C_8H_{12}O_6$.

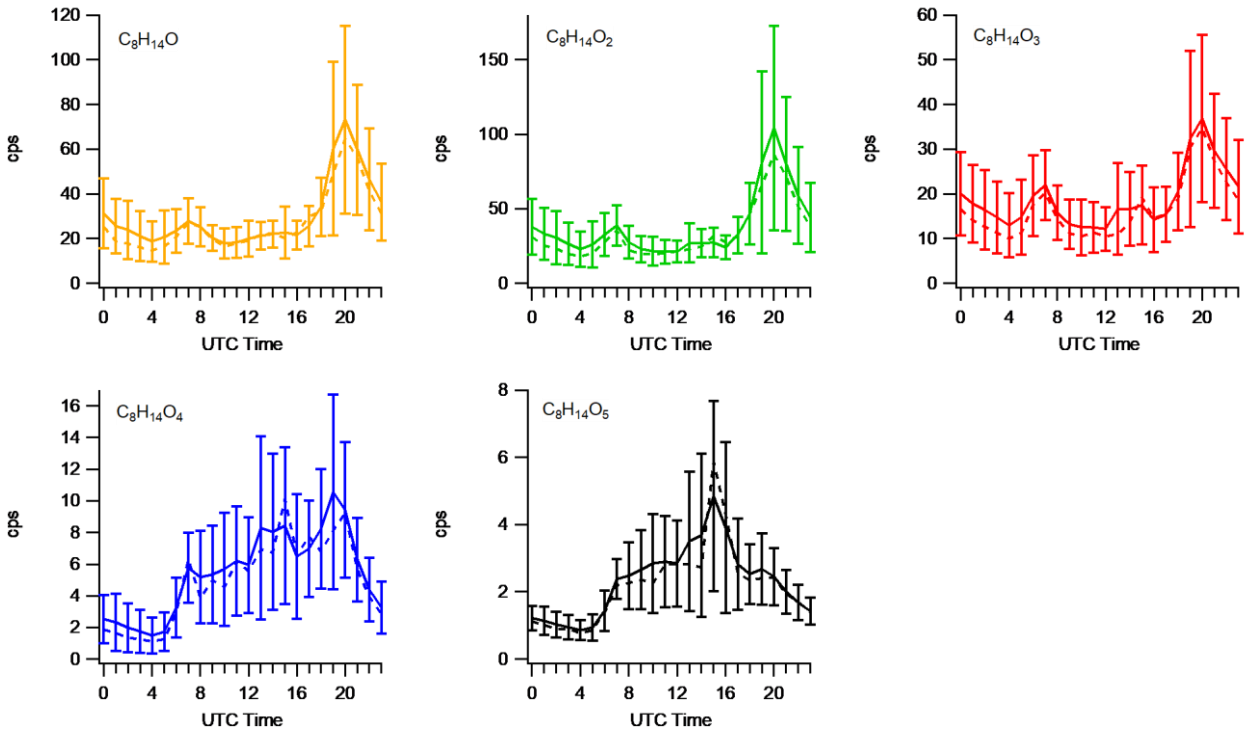

Figure S9. Diurnal patterns of non-nitrate monoterpene oxidation products: (a) $C_8H_{14}O$, (b) $C_8H_{14}O_2$, (c) $C_8H_{14}O_3$, (d) $C_8H_{14}O_4$, and (e) $C_8H_{14}O_5$.

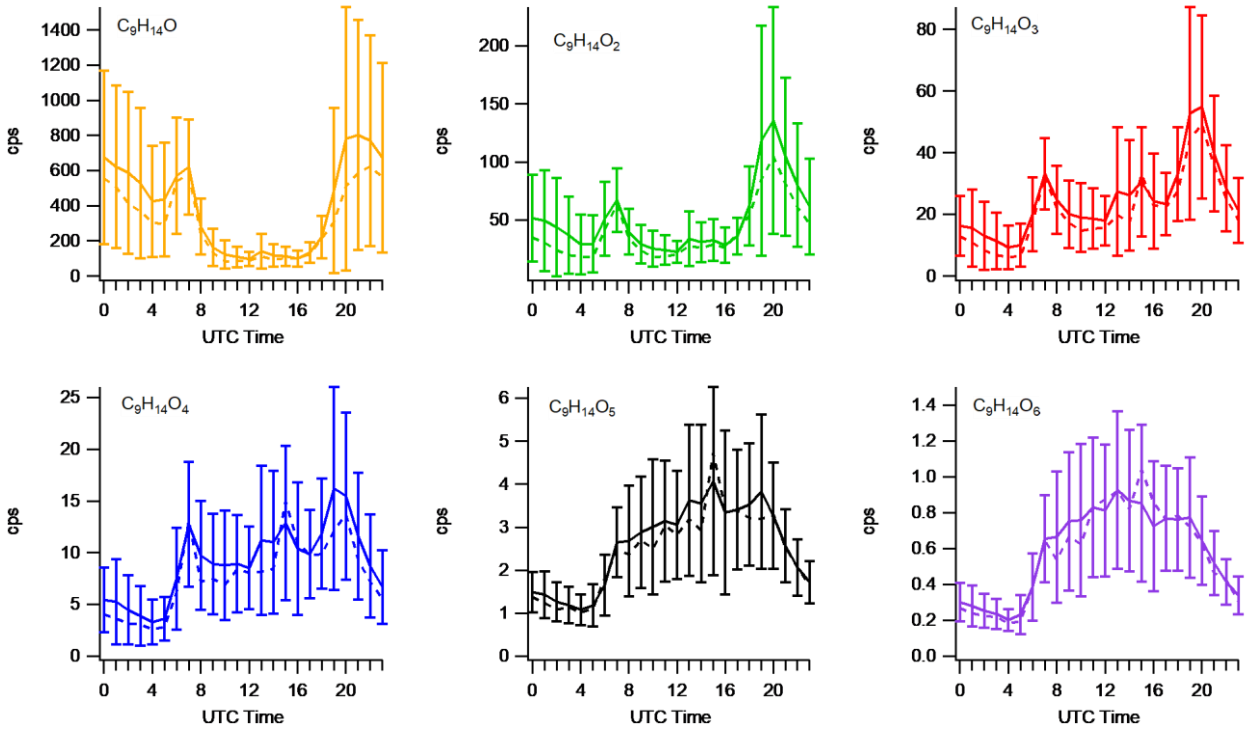

Figure S10. Diurnal patterns of non-nitrate monoterpene oxidation products: (a) $C_9H_{14}O$, (b) $C_9H_{14}O_2$, (c) $C_9H_{14}O_3$, (d) $C_9H_{14}O_4$, (e) $C_9H_{14}O_5$, and (f) $C_9H_{14}O_6$.

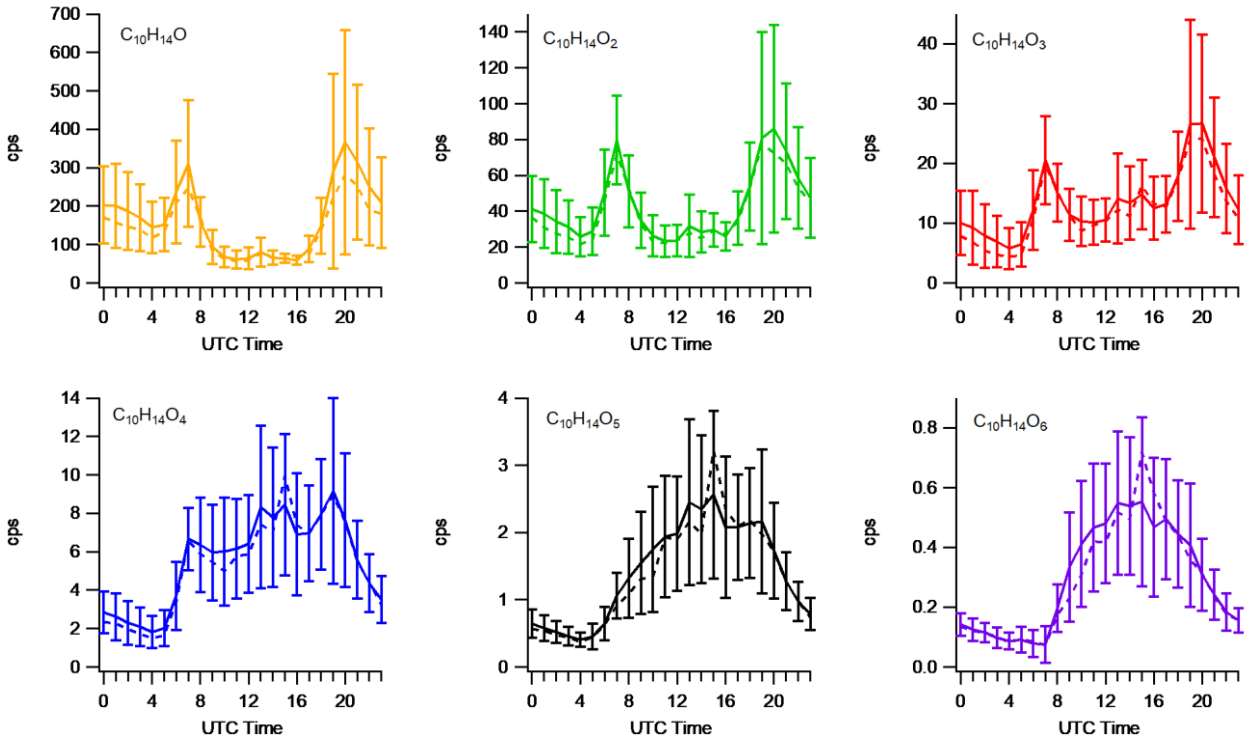

Figure S11. Diurnal patterns of non-nitrate monoterpene oxidation products: (a) $C_{10}H_{14}O$, (b) $C_{10}H_{14}O_2$, (c) $C_{10}H_{14}O_3$, (d) $C_{10}H_{14}O_4$, (e) $C_{10}H_{14}O_5$, and (f) $C_{10}H_{14}O_6$.

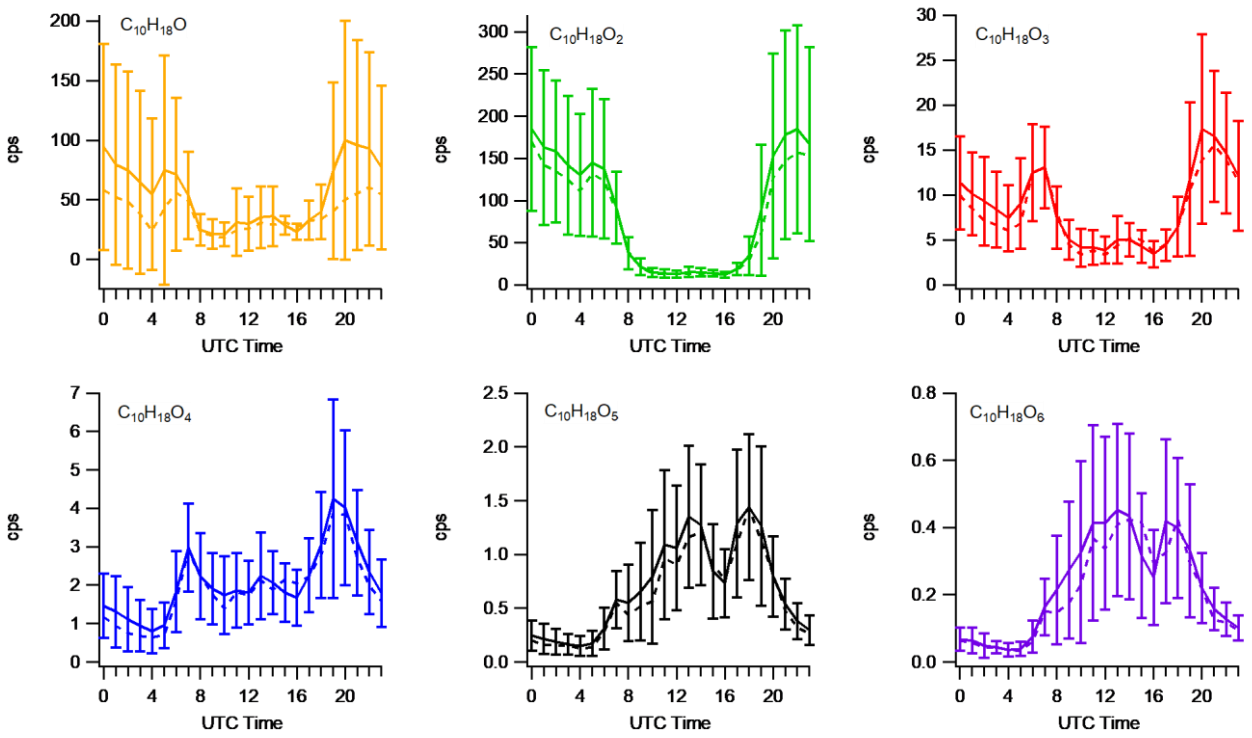

Figure S12. Diurnal patterns of non-nitrate monoterpene oxidation products: (a) $C_{10}H_{18}O$, (b) $C_{10}H_{18}O_2$, (c) $C_{10}H_{18}O_3$, (d) $C_{10}H_{18}O_4$, (e) $C_{10}H_{18}O_5$, and (f) $C_{10}H_{18}O_6$.

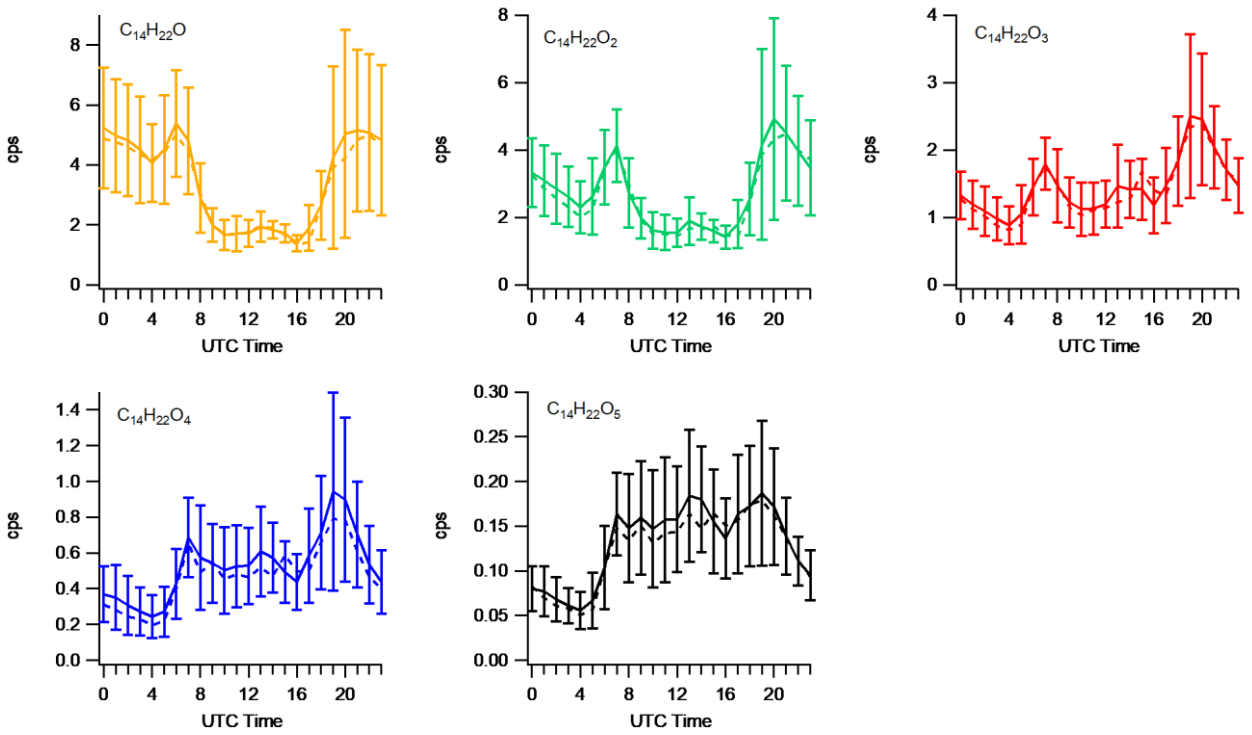

Figure S13. Diurnal patterns of non-nitrate sesquiterpene oxidation products: (a) $C_{14}H_{22}O$, (b) $C_{14}H_{22}O_2$, (c) $C_{14}H_{22}O_3$, (d) $C_{14}H_{22}O_4$, and (e) $C_{14}H_{22}O_5$.

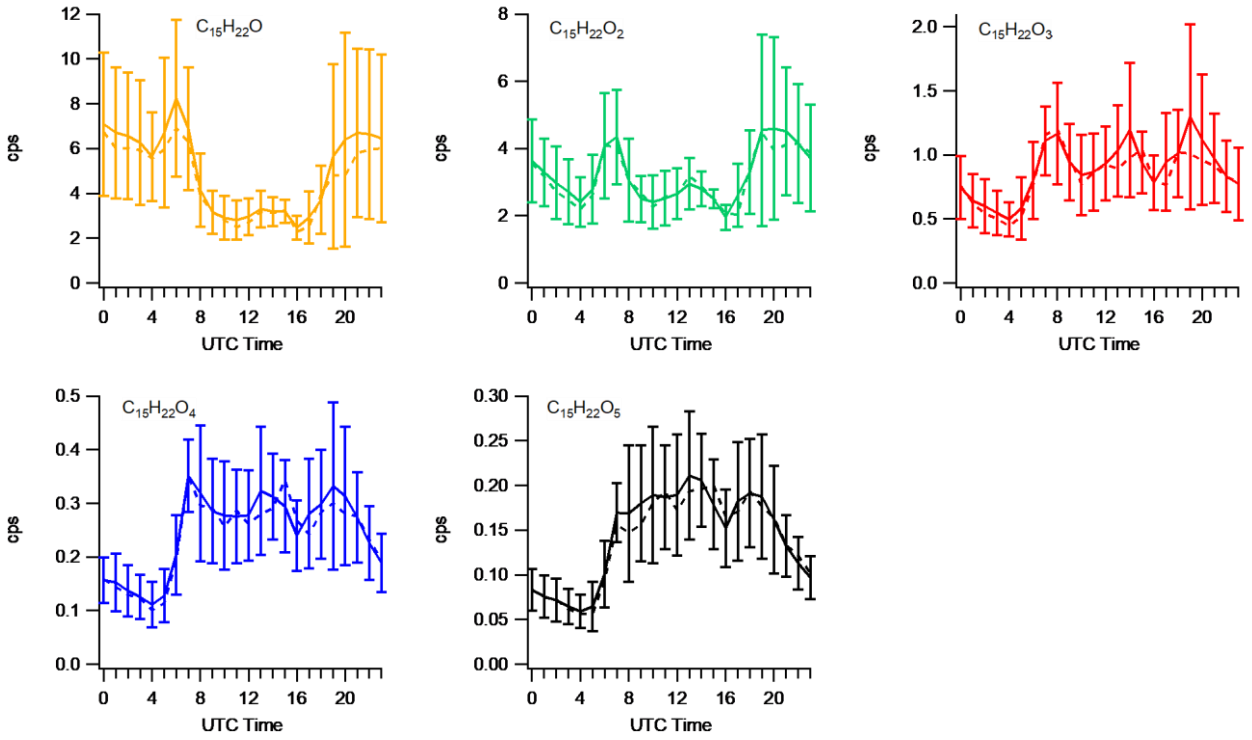

Figure S14. Diurnal patterns of non-nitrate sesquiterpene oxidation products: (a) $C_{15}H_{22}O$, (b) $C_{15}H_{22}O_2$, (c) $C_{15}H_{22}O_3$, (d) $C_{15}H_{22}O_4$, and (e) $C_{15}H_{22}O_5$.

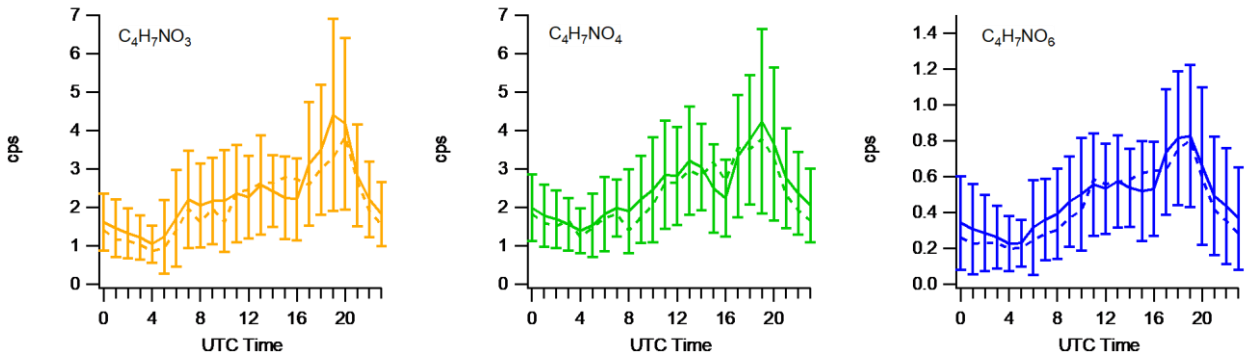

Figure S15. Diurnal patterns of isoprene-derived organic nitrates: (a) $C_4H_7NO_3$, (b) $C_4H_7NO_4$, and (c) $C_4H_7NO_6$.

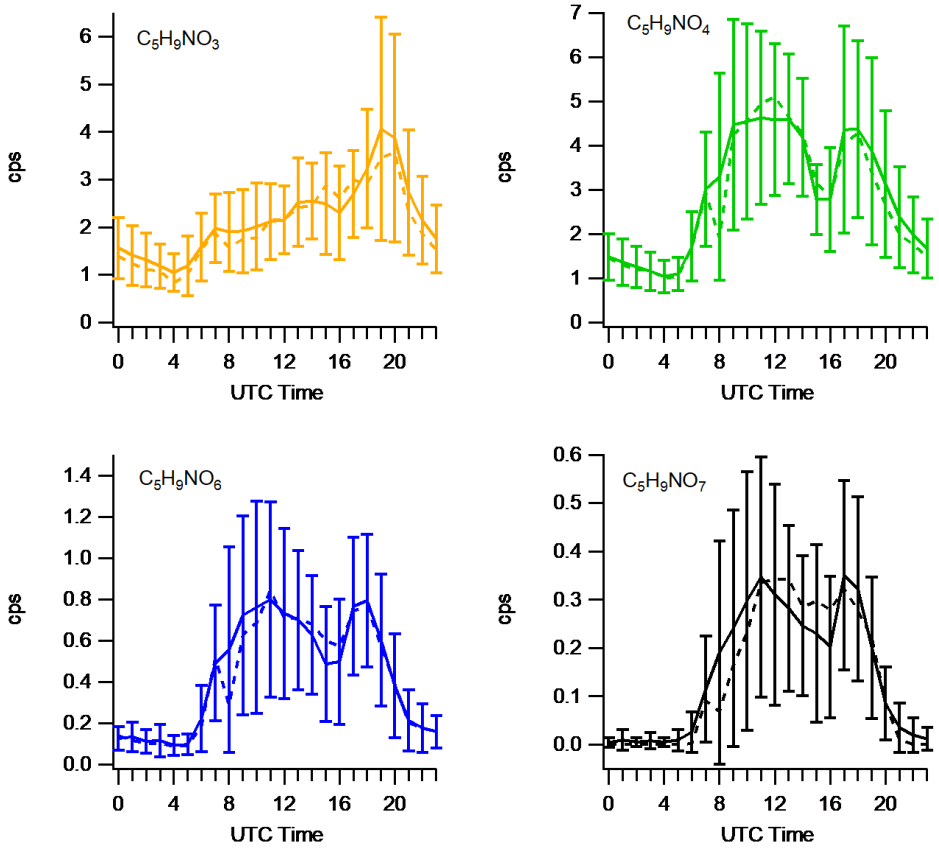

Figure S16. Diurnal patterns of isoprene-derived organic nitrates: (a) $C_5H_9NO_3$, (b) $C_5H_9NO_4$, (c) $C_5H_9NO_6$, and (d) $C_5H_9NO_7$.

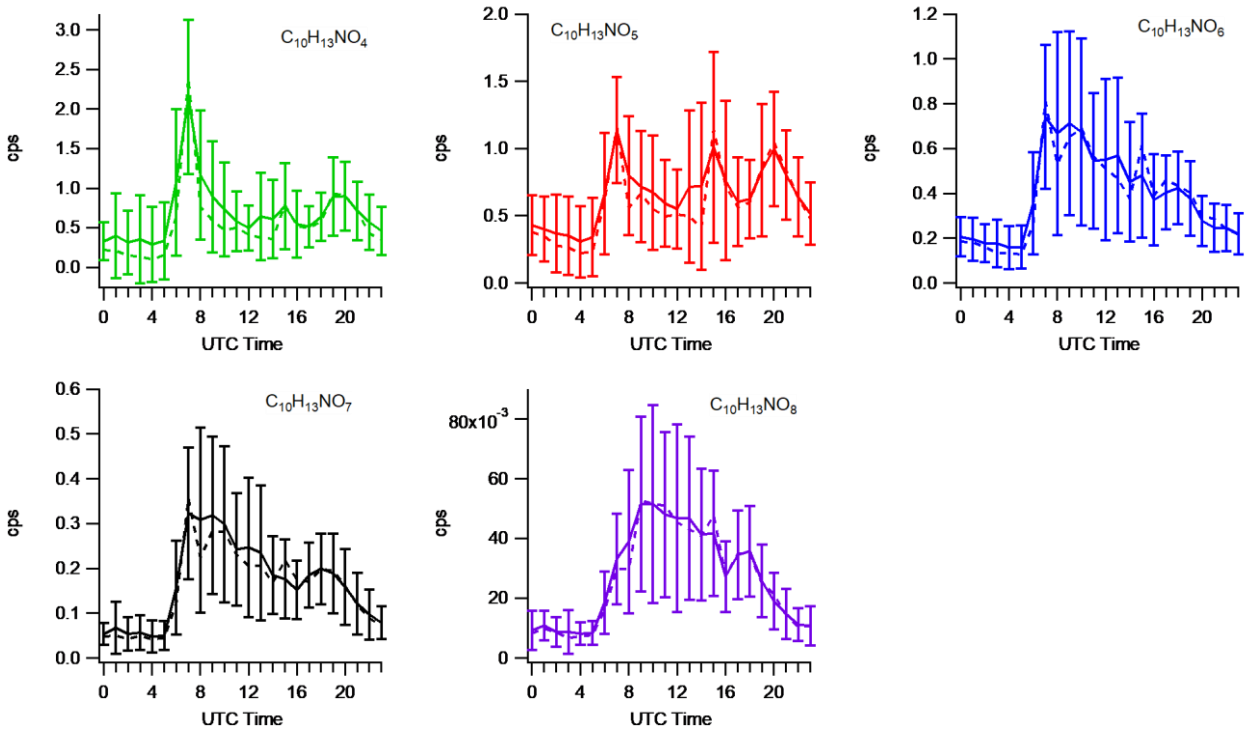

Figure S17. Diurnal patterns of monoterpene-derived organic nitrates: (a) $C_{10}H_{13}NO_4$, (b) $C_{10}H_{13}NO_5$, (c) $C_{10}H_{13}NO_6$, (d) $C_{10}H_{13}NO_7$, and (e) $C_{10}H_{13}NO_8$.

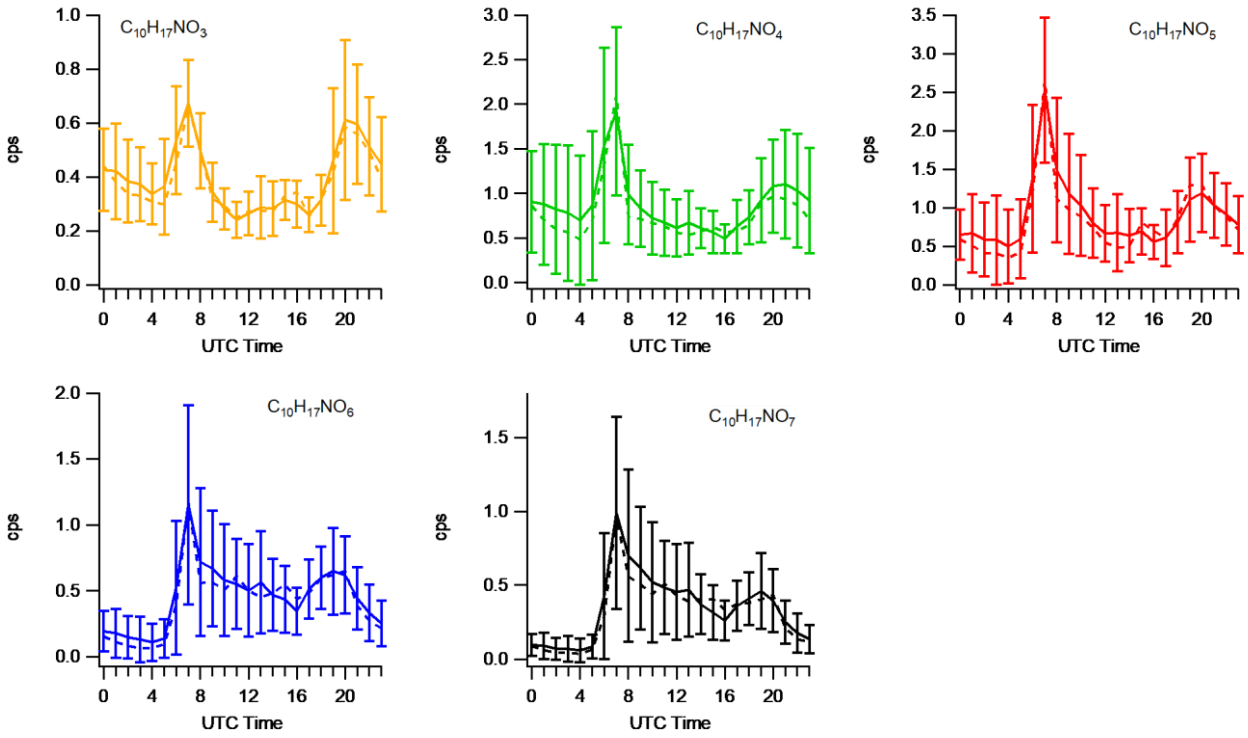

Figure S18. Diurnal patterns of monoterpene-derived organic nitrates: (a) $C_{10}H_{17}NO_3$, (b) $C_{10}H_{17}NO_4$, (c) $C_{10}H_{17}NO_5$, (d) $C_{10}H_{17}NO_6$, and (e) $C_{10}H_{17}NO_7$.

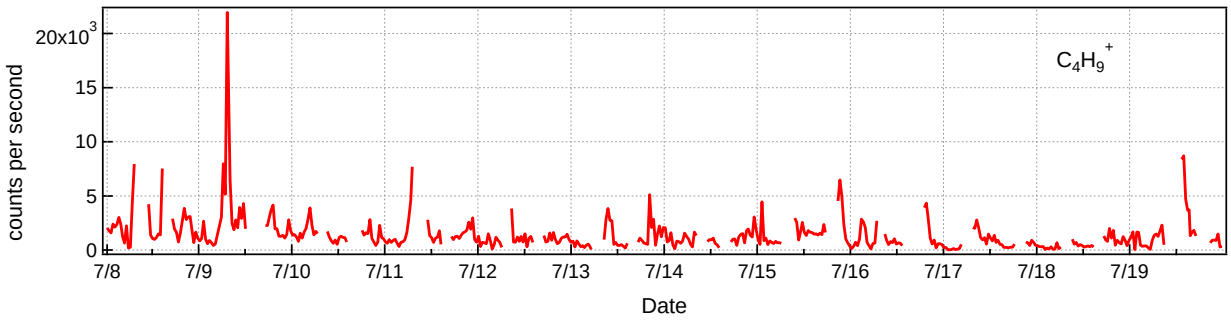

Figure S19. Time series of the identified $C_4H_9^+$.